Poly(ether amide) Segmented Block Copolymers with Adipic Acid Based Tetraamide Segments

G. J. E. Biemond,* J. Feijen, R. J. Gaymans

Department of Science and Technology, University of Twente, P.O. Box 217, 7500 AE, Enschede, The Netherlands

Received 10 October 2006; accepted 11 January 2007
DOI 10.1002/app.26202
Published online 6 April 2007 in Wiley InterScience (www.interscience.wiley.com).

ABSTRACT: Poly(tetramethylene oxide)-based poly(ether ester amide)s with monodisperse tetraamide segments were synthesized. The tetraamide segment was based on adipic acid, terephthalic acid, and hexamethylenediamine. The synthesis method of the copolymers and the influence of the tetraamide concentration, which was varied between 3 and 44 wt %, were studied. The copolymers were characterized by differential scanning calorimetry and temperature-dependent Fourier transform infrared, small-angle X-ray scattering, atomic force microscopy, and dynamic mechanical thermal analysis. The monodisperse tetraamide segments crystallized fast, forming crystalline ribbons with high aspect ratios, and the crystallinity of the tetraamide segments in the copolymers was typically 90%. The glass-transition temperature of the poly(tetramethylene oxide) phase was low (−65 to −70°C), and the modulus in the plateau region of the copolymers was virtually temperature-independent. With increasing content of crystallizable amide segments in the copolymer, the storage modulus at room temperature increased from 1 to 102 MPa. This strong increase in the modulus with the tetraamide content could be approximated with a model for fiber-reinforced polymers. © 2007 Wiley Periodicals, Inc. J Appl Polym Sci 105: 951–963, 2007

Key words: block copolymers; elastomers; macromonomers; mechanical properties; molecular reinforcement

INTRODUCTION

Thermoplastic elastomers are melt-processable materials that have elastomeric behavior at their service temperature. Segmented copolymers that consist of alternating rigid and flexible segments constitute a special kind of thermoplastic elastomer.[1,2] The rigid segments can crystallize in lamellae (ribbons) that are dispersed in the low glass-transition temperature (T_g) phase. These crystallites function as physical crosslinks reinforcing the matrix, thus giving the material dimensional stability and solvent resistance. The soft, low-T_g phase forms the continuous phase and gives the material low temperature flexibility. The T_g of the soft phase depends on the glass transition of the flexible segment, the segment length between physical crosslinks, and the amount of dissolved rigid segments.[1,2] At room temperature, the copolymers display low moduli and interesting elastic behavior. For a wide rubbery plateau, the T_g of the soft phase should be low, and the melting temperature (T_m) of the hard phase should be high. Poly(tetramethylene oxide) (PTMO) is often used as the flexible segment as it has a low T_g, good hydrolytic stability, good reactivity, and strain-hardening behavior.[3] The molecular weight of the available PTMO segments is limited, and high-molecular-weight polyether segments can be obtained by the extension of $PTMO_x$ with terephthalate units [$(PTMO_x–T)_y$].[4,5] Such an extension of the PTMO segments causes the T_g of the polyether phase to increase only slightly (5°C).

The crystallization of the rigid segments is considerably improved when the segments are monodisperse in length.[4–18] Segmented block copolymers with monodisperse crystallizable segments have been studied for polyurethanes,[6–12] and polyamides.[4,5,13–18] These studies have shown that polymers with monodisperse crystallizable segments crystallize fast and have low T_g's, relatively high moduli, temperature-independent rubbery plateaus, high elasticities, and high fracture strains. When monodisperse amide segments are used, these segments are often synthesized before the polymerization. Very suitable segments are the completely aromatic diamides[4,16,17] and the partially aromatic tetraamides based on polyamide 6T (T6T6T).[5,13,18] The wholly aromatic dimethyl ester/diamide segments have a high T_m (371°C), as do the partially aromatic dimethyl ester tetraamides (∼ 300°C).[13,19] Such T_m's are too high for a melt polymerization. Furthermore, copolymers with these diamide and tetraamide segments at high amide contents (> 35 wt %) have T_m's above 240°C, which is too high for degradation-free processing. A bisester tetraamide unit that is less

**Present address:* Sabic-Europe, Geleen, The Netherlands.
Correspondence to: R. J. Gaymans (r.j.gaymans@tnw.utwente.nl).

Contract grant sponsor: Dutch Polymer Institute; contract grant number: 137.

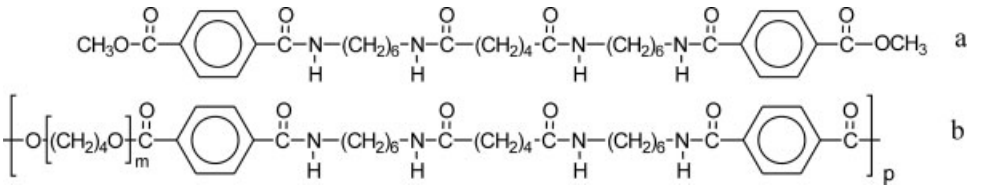

Figure 1 Structures of (a) T6A6T-dimethyl and (b) the PTMO–T6A6T copolymer.

aromatic is expected to have a lower T_m. Such a bisester tetraamide is T6A6T-dimethyl (Fig. 1), which is based on the bulk chemicals hexamethylenediamine (HMDA or 6), terephthalic acid (T), and adipic acid (A). With the T6A6T-dimethyl units, segmented block copolymers are made with monodisperse crystallizable tetraamide segments.

This study concerns the synthesis of T6A6T-dimethyl units and segmented copolymers $PTMO_x$–T6A6T and $(PTMO_{1000}–T)_y$–T6A6T. In the copolymers, the $PTMO_x$ length was varied from 650 to 2900 g/mol, and the $(PTMO_{1000}–T)_y$ length was varied from 1000 to 20,000 g/mol; this implied a variation in the concentration of the tetraamide segment from 44 to 2.7 wt %. The amide crystallization was studied with differential scanning calorimetry (DSC) and Fourier transform infrared (FTIR), and the morphology was studied by atomic force microscopy (AFM) and small-angle X-ray scattering (SAXS). The thermal mechanical behavior was studied with dynamic mechanical thermal analysis (DMTA).

EXPERIMENTAL

Materials

Dimethyl terephthalate (DMT), *N*-methyl-2-pyrrolidone (NMP), phenol, terephthaloyl chloride, toluene, and a 0.5*M* sodium methoxide solution in methanol were purchased from Aldrich (Mijdrecht, The Netherlands) and used as received. Tetraisopropyl orthotitanate [Ti(i-$OC_3H_7)_4$] was also purchased from Aldrich and was diluted with *m*-xylene (0.05*M*), which was purchased from Merck (Haarlem, The Netherlands). PTMO 632 was donated by Bayer (Leverkusen, Germany), and PTMO samples with molecular weights of 1000, 1400, 2000, and 2900 g/mol were donated by DuPont (Geneve, Switzerland). Irganox 1330 was obtained from Ciba (Basel, Switzerland). Methyl phenyl terephthalate (MPT) was synthesized from monomethyl terephthalate, as described previously,[5] and the synthesis procedure of diphenyl terephthalate (DPT) from terephthaloyl chloride can be found in detail elsewhere.[5,15]

Synthesis of bis(6-amino hexamethylene)adipamide (6A6-diamine)

1,6-Hexamethylenediamine (500 g, 4.3 mol) was melted in a round-bottom flask, and dimethyl adipate (53 g, 0.3 mol) was added. Sodium methoxide (6 mL of a 0.5*M* solution in methanol) was used as a catalyst. The reaction was performed at 75°C for 16 h, and after cooling, the product was collected over a no. 4 filter and washed twice with diethyl ether. 6A6 was recrystallized from hot 1,4-dioxane (16 g/L) at 100°C. The purity was determined with eq. (1):

$$\text{Purity of 6A6 (\%)} = \left(2 - \frac{\text{Integral CH}_2\text{ amide side } (\delta 3.56)}{\text{Integral CH}_2\text{ amine side } (\delta 3.28)}\right) \times 100\% \quad (1)$$

Synthesis of T6A6T-dimethyl

A mixture of 6A6-diamine (34 g, 0.1 mol) and MPT (77 g, 0.3 mol) was dissolved in 1 L of NMP and heated to 120°C for 16 h. After cooling, the precipitated reaction product was collected on a glass filter and washed with NMP, toluene, and acetone consecutively. The purity of T6A6T-dimethyl was determined with eq. (2), assuming that the used 6A6 was pure:

$$\text{Purity of T6A6T} - \text{dimethyl (\%)} = \left(2 - \frac{\delta\ 7.8\text{–}8.0}{\delta\ 8.2\text{–}8.3}\right) \times 100\% \quad (2)$$

The purity of T6A6T was 98%, and the yield was 83%.

Solution/melt polymerization of $PTMO_x$–T6A6T

The polymerization of $PTMO_{1000}$ with T6A6T-dimethyl is given as an example. The polymerization was carried out in a 250-mL, stainless steel reactor with a nitrogen inlet and a magnetic coupling stirrer. The reactor was charged with $PTMO_{1000}$ (50 g, 0.05 mol), T6A6T-dimethyl (33.3 g, 0.05 mol), 100 mL of NMP, 1 wt % Irganox 1330 (based on PTMO), and a catalyst solution [5 mL of 0.05*M* Ti(i-$OC_3H_7)_4$ in *m*-xylene] under a nitrogen flow. The stirred reaction mixture was heated to 180°C during a period of 30 min and then to 250°C during a period of 2 h and finally maintained at 250°C for 2 h. Subsequently, the pressure was carefully reduced (<20 mbar) to distill off the NMP and then further reduced (<0.3 mbar) for 1 h. After this, the reactor was cooled slowly, maintaining the low pressure. The copolymers were transparent and tough materials.

^{1}H-NMR [deuterated trifluoro acid (TFA-*d*)]: δ 8.35 (d, 4H, terephthalate H ester side), δ 8.00 (d, 4H, terephthalate amide side), δ 4.6 (s, 4H, CH_2 PTMO, ester side), δ 3.88 (m, 52H, CH_2 PTMO ether side), δ 2.87 (t, 4H, first and fourth CH_2 methyl adipate), δ 2.07 (t, 8H, CH_2 PTMO, ester side), δ 1.91 (s, 48H, CH_2 PTMO) + δ 1.9 (d, 4H, second and third CH_2 methyl adipate), δ 1.78 (s, 8H, second and fifth CH_2 amine), δ 1.63 (s, 8H, 3rd and 4th CH_2 amine).

Melt polymerization of PTMO$_x$–T6A6T

For the melt polymerization of PTMO$_x$–T6A6T, the same setup described previously was used. The reactor was charged with $PTMO_{2900}$ (50 g, 0.017 mol), T6A6T-dimethyl (11.48 g, 0.017 mol), 1 wt % Irganox 1330 (based on PTMO), and a catalyst solution [2 mL of 0.05*M* Ti(i-OC_3H_7)$_4$ in *m*-xylene] under a nitrogen flow. The initial reaction temperature was 260°C, which was 10°C higher than the T_m of the bisester tetraamide unit. After 30 min, the tetraamide unit was melted, and the reaction temperature was lowered to 250°C. This temperature was maintained for 4 h. Subsequently, the pressure was reduced to < 20 mbar and then further to < 0.3 mbar for 1 h. Finally, the reactor was cooled slowly, maintaining the low pressure. The copolymers were transparent and tough.

Solution/melt polymerization of PTMO$_x$–T6A6T starting from 6A6/DPT

A setup equivalent to the ones described previously was used for the solution/melt polymerization. The reactor was charged with $PTMO_{1400}$ (50 g, 0.036 mol), DPT (17 g, 0.054 mol), 1 wt % Irganox 1330 (based on PTMO), and a catalyst solution [0.9 mL of 0.05*M* Ti(i-OC_3H_7)$_4$ in *m*-xylene] under a nitrogen flow. After 2 h of reaction at 220°C, a solution of 6A6-diamine (6.11 g, 0.018 mol) in 50 mL of NMP was added to the reactor. The temperature was raised to 250°C and maintained there for 2 h. Subsequently, the pressure was carefully reduced (< 20 mbar) to distill off the NMP and then further reduced (< 0.3 mbar) for 60 min. Finally, the reactor was cooled slowly, maintaining the low pressure. The copolymers were tough and had a yellowish color.

^{1}H-NMR

NMR spectra were recorded with a Bruker AC 300 spectrometer at 300 MHz. TFA-*d* was used as the solvent.

Viscometry

The solution viscosities were measured at a concentration of 0.1 g/dL in a mixture of phenol and 1,1,2,2-tetrachloroethane (1 : 1 molar ratio) at 25°C with an Ubbelohde-type 1B capillary, and from these, the inherent viscosities were calculated. The value of the inherent viscosity approached that of the intrinsic viscosity.[20]

DSC

DSC (Perkin-Elmer, Monza, Italy) thermograms were recorded on a PerkinElmer DSC apparatus equipped with a PE7700 computer and TAS-7 software and calibrated with indium. Dried samples of 5–10 mg were heated to approximately 30°C above the T_m, subsequently cooled, and then heated again. Both the heating and cooling rates were 20°C/min. The crystallization temperature (T_c) was taken as the onset of crystallization in the first cooling scan. The maximum of the peak in the second heating scan was taken as T_m, and the melting enthalpy also could be determined from this peak. The degree of crystallinity was calculated from the melting enthalpy of the polymer and the melting enthalpy of the bisester tetraamide.

FTIR

IR transmission spectra were recorded with a Nicolet 20SXB FTIR (Nicolet, Cambridge, MA) spectrometer with a resolution of 4 cm^{-1}. Samples measured at room temperature were prepared by the addition of a droplet of a polymer solution in hexafluoroisopropanol (HFIP) (1 g/L) to a pressed KBr pellet. Solution-cast polymer films (0.05 g/mL in HFIP) of < 10-μm thickness, placed between two KBr pellets, were used for temperature-dependent FTIR measurements. These were recorded at temperatures between room temperature and 210°C under a helium flow. The degree of crystallinity of the rigid segments in the polymers (X_c) was estimated with the following equations [eqs. (3) and (4)]:

$$X_c \text{ by FTIR} = \frac{\text{Crystalline amide peak}}{\text{Amorphous} + \text{Crystalline amide peak}} = \frac{\lambda_{25^\circ\text{C}(1630\ \text{cm}^{-1})}}{a \times \lambda_{25^\circ\text{C}(1670\ \text{cm}^{-1})} + \lambda_{25^\circ\text{C}(1630\ \text{cm}^{-1})}} \quad (3)$$

where λ_T is the height of the absorption band at temperature T (°C).

The heights of the amorphous and crystalline amide peaks are related by the factor a, which can be calculated according to

$$a = \frac{\text{Decrease of crystalline peak}_{(25^\circ\text{C}-\text{melt})}}{\text{Increase of amorphous peak}_{(25^\circ\text{C}-\text{melt})}} = \frac{\lambda_{25^\circ\text{C}(1630\ \text{cm}^{-1})} - \lambda_{\text{melt}(1630\ \text{cm}^{-1})}}{\lambda_{\text{melt}(1670\ \text{cm}^{-1})} - \lambda_{25^\circ\text{C}(1670\ \text{cm}^{-1})}} \quad (4)$$

AFM

AFM (Vieco, Breda, The Netherlands) measurements were carried out with a Nanoscope IV controller (Veeco) operating in a tapping mode. Si cantilevers (Veeco) were used to obtain height and phase images. The amplitude in the free oscillation was 5.0 V. The operating set-point value (A/A_0) was set to relatively low values of 0.70, the scale for the phase angle was 0–20°, and the size of the scans was 1 × 1 μm. Solvent-cast samples with thicknesses of ~ 20 μm were prepared on silicon wafers from a 3 wt % solution in TFA.

Synchrotron wide-angle X-ray scattering (WAXS) and SAXS

WAXS and SAXS experiments were performed on Dutch–Belgium beam line BM26 at the European Synchrotron Radiation Facility in Grenoble, France. The wavelength of the beam was 1.2 Å. For the WAXS experiments, a one-dimensional detector was used, and the measurements were carried out in a 2θ-range of 9.3–70°. For the SAXS measurements, the detector was two-dimensional, and the scattering vector (q) range was 0–1.8 nm^{-1}. Temperature-dependent profiles were recorded with a Linkam (Polett, Texas) remote-controlled DSC stage at a heating and cooling rate of 10°C/min. The background was subtracted from the intensity. The two-dimensional SAXS intensity was azimuthally integrated to obtain the scattering pattern as a function of $q = 4\pi \sin \theta/\lambda$. The samples were placed in DSC pans, and small holes were pierced in the bottom and top of the pans to increase the intensity of the signal. Mica film was used to cover the holes to keep the molten sample in the DSC pan.

The long spacing [L (nm)] was calculated with eq. (5):

$$L = \frac{2\pi}{q} \tag{5}$$

DMTA

Samples (70 × 9x2 mm) for the DMTA measurements were prepared on an Arburg (Slossburg, Germany) H manual injection-molding machine at a barrel temperature that was set 20°C higher than the T_m of the copolymer. The test samples were dried *in vacuo* at 50°C for 24 h before analysis. DMTA thermograms were recorded with a Myrenne (Aachen, Germany) ATM3 torsion pendulum at a frequency of 1 Hz and 0.1% strain. The storage modulus (G') and loss modulus (G'') were measured as functions of temperature. The samples were cooled to −100°C and subsequently heated at a rate of 1°C/min. The temperature at the maximum of the G'' peak was taken as T_g. The flow temperature (T_{flow}) was defined as the temperature at which G' reached 1 MPa. The start of the rubbery plateau, that is, the intercept of the tangents, was denoted the flex temperature (T_{flex}). The decrease in G' of the rubbery plateau with increasing temperature can be quantified by $\Delta G'$ ($^\circ C^{-1}$), which is calculated with eq. (6):

$$\Delta G' = \frac{G'_{(\mathrm{Tflex})} - G'_{(\mathrm{Tflow-50^oC})}}{G'_{25^oC}} \times \frac{1}{\Delta T} \tag{6}$$

where ΔT is the temperature range [(T_{flow} − 50°C) to T_{flex}].

Compression set (CS)

The samples for CS were cut from the injection-molded bars. The CS was measured according to the ASTM 395 B standard. A compression of 25% was maintained for 24 h at room temperature and was then released. After an additional 30 min, the thicknesses of the samples were measured. The CS was taken as the average of three measurements and is defined according to eq. (7):

$$\mathrm{CS} = \frac{d_0 - d_2}{d_0 - d_1} \times 100\% \tag{7}$$

where d_0 is the thickness before the compression (mm), d_1 is the compressed thickness (mm; here d_1 = 1.65 mm), and d_2 is the thickness 30 min after the release of the compression (mm).

RESULTS AND DISCUSSION

Copolymers based on T6A6T-dimethyl and $PTMO_x$ or $PTMO_{1000}$ extended with terephthalate groups [$PTMO_{1000}$–T)$_y$] were synthesized via polycondensation reactions. The bisester tetraamide T6A6T-dimethyl and the diamine–diamide 6A6 were synthesized before the polymerization.

Synthesis of T6A6T-dimethyl

The uniform T6A6T-dimethyl units were prepared in two steps (Fig. 2). In the first step, 6A6-diamine units were synthesized by the reaction of dimethyl adipate

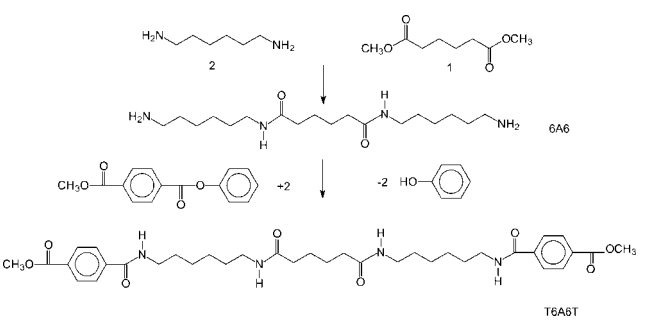

Figure 2 Synthesis of T6A6T-dimethyl.

with an excess of HMDA. Although an excess of diamine was employed, longer blocks were still formed. The 6A6 was recrystallized from dioxane. The ^{1}H-NMR (TFA-*d*) spectrum had the following peaks: δ 8.2–8.3 (4H, terephthalic ester side), δ 7.8–8.0 (4H, terephthalic amide side), δ 4.1, (6H, methyl ester), δ 3.7–3.8 (4H, CH_2 amine terephthalamide), δ 3.7–3.8 (4H, CH_2 amine adipamide), δ 2.7–2.8 (4H, CH_2 acid adipamide), δ 1.92 (4H, CH_2 adipamide mid), and δ 1.53–1.92 (6H, CH_2 HMDA mid). Before recrystallization, both the yield and purity were 85%. After recrystallization, on the other hand, the yield and purity were 63 and 98%, respectively. DSC determined T_m to be 183°C and heat of melting (ΔH_m) to be 33 J/g.

The second step involved the synthesis of T6A6T-dimethyl from 6A6-diamine and methyl phenyl terephthalate (MPT). Of MPT, the phenyl ester is far more reactive compared with the methyl ester, and thus further reaction was limited. The purity of the bisester tetraamides was determined by ^{1}H-NMR and was found to be 98%. As studied by DSC, the T6A6T-dimethyl had a single T_m value of 255°C and a ΔH_m value of 138 J/g, as well as a single T_c value at 235°C and a heat of crystallization (ΔH_{cr}) value of 111 J/g.

The IR spectrum of T6A6T is given in Figure 3, and the relevant bands are in the regions of 1600–1700 (amide I), 1700–1750 (ν C=O ester), and 3200–3500 cm^{-1} (ν N—H). Two bands for amide I can be seen in the figure: one is for the aliphatic amide (1640 cm^{-1}), and the other is for the aromatic amide band (1630 cm^{-1}).[21] The amorphous amide I band is expected at 1660–1670 cm^{-1}. The ester carbonyl is at 1720 cm^{-1}, and the hydrogen-bonded νNH is at 3300 cm^{-1}.

Figure 4 displays the change in the FTIR spectrum on melting, and it can be seen that the amide I bands at 1630–1640 cm^{-1} and the νNH at 3300 cm^{-1} are sensitive to this phenomenon. The peaks at 1630–1640 cm^{-1} disappeared, and a broad peak at

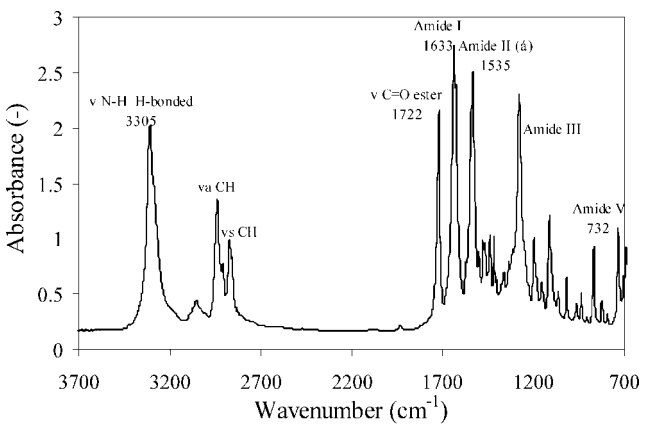

Figure 3 FTIR spectrum of T6A6T-dimethyl at 25°C.

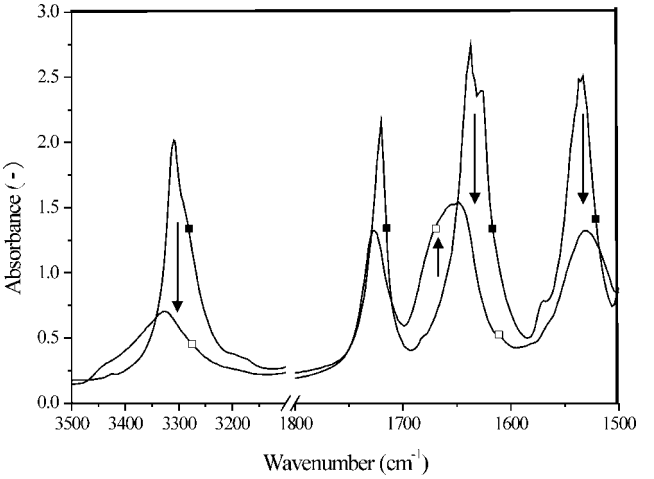

Figure 4 FTIR spectra of T6A6T-dimethyl at (■) 25 and (□) 260°C.

1670 cm^{-1} (ν C=O amorphous) was formed. The νN—H band at 3300 cm^{-1} decreased, and a small, broad peak at 3400 cm^{-1} was formed, corresponding to non-hydrogen-bonded N—H groups. At temperatures above 260°C, a small peak at 3320 cm^{-1} is seen, suggesting that some association of H-bonded assemblies was still present in the melt.

The WAXS pattern of T6A6T-dimethyl has spacings at 12.6 (0.28 nm), 14.4 (0.24 nm), 14.7 (0.24 nm), and 15.9° (0.22 nm; Fig. 5). When the temperature increased, the peak at 12.6° shifted to lower angles, whereas the peaks at 14.4, 14.7, and 15.9° shifted to higher angles. This suggests a decrease in the length in the chain direction, whereas the dimensions increased in the cross section. Above the T_m of T6A6T-dimethyl (> 255°C), only a broad, amorphous peak is observed, with its maximum at 14.5° (0.42 nm). This indicates that no liquid-crystalline order was present in the molten phase. At room temperature, an amorphous peak is barely present in the

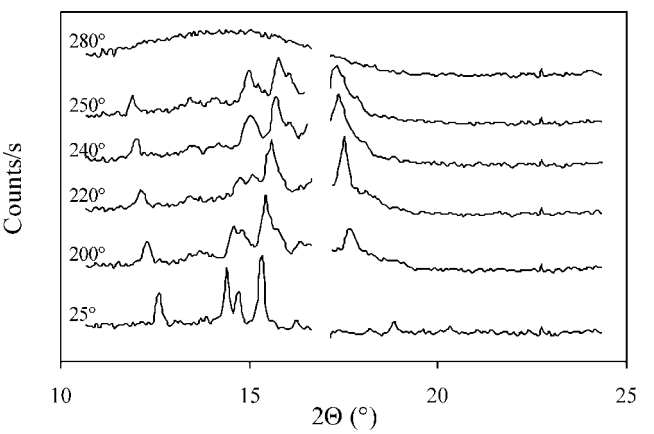

Figure 5 WAXS patterns for T6A6T-dimethyl with increasing temperatures.

TABLE I
Synthesis Methods for PTMO–T6A6T (∼ 15 wt % T6A6T)

	Polymerization type	Inherent viscosity (dL/g)	T_g (°C)	$G'_{25°C}$ (MPa)	$\Delta G' \times 10^{-3}$ (°C^{-1})	T_{flow} (°C)	CS (%)	Appearance
T6A6T-dimethyl + $PTMO_{2900}$	Melt	2.1	−71	6	3.7	150	14	Transparent
T6A6T-dimethyl + $PTMO_{2900}$	Solvent/melt	3.5	−70	9	1.8	175	7	Transparent
6A6 + (DPT + $PTMO_{1400}$)$_{3060}$	Solvent/melt	1.6	−60	8	4.1	165	14	Opaque

pattern, and thus the crystallinity of the T6A6T-dimethyl units must be high.

Polymerization method

The influence of the polymerization method on the properties of the PTMO–T6A6T copolymers was studied. It was found that the use of NMP as a solvent in the presence of a titanate catalyst resulted in a coloring of the copolymer (unpublished results).

Melt polymerization

The copolymers were prepared by the reaction of the methyl ester end groups of T6A6T-dimethyl with the hydroxyl end groups of the $PTMO_{2900}$ segment. During melt polymerization, the bisester tetraamide unit needs to melt and mix with the $PTMO_{2900}$. Thus, the initial temperature during polymerization should be more than 5°C higher than the T_m of the bisester tetraamide unit (255°C). An initial temperature of 260°C was chosen, but once the reaction was under way, the polymerization temperature was lowered to 250°C for the remainder of the reaction. This was done to avoid degradation of the polyether segment as a result of the high polymerization temperature.[22] The melt-synthesized copolymer $PTMO_{2900}$–T6A6T with ∼ 15 wt % T6A6T was transparent and only slightly colored. The inherent viscosity of this copolymer was high (2.1 dL/g), the storage modulus at room temperature ($G'_{25°C}$) was 6 MPa, and the T_m was 150°C (Table I). The CS was 14%.

Solution/melt polymerization

By the use of a solvent in the initial part of the solution/melt polymerization, the temperature could be kept low. NMP was used to dissolve T6A6T-dimethyl, and as soon as the T6A6T-dimethyl was incorporated into the copolymer, the T_m was increased to 250°C, and the NMP was stripped. The reaction was subsequently continued in the melt at 250°C. The $PTMO_{2900}$–T6A6T copolymer obtained in this way had a very high inherent viscosity (3.5 dL/g; Table I). The copolymer had a higher T_{flow}, a higher rubber modulus, and a lower CS but was more yellow-colored than the melt-synthesized material. The copolymer obtained with this solution/melt polymerization process thus had better properties than the melt-synthesized one. With this method, the viscosities were higher, probably because of a lower initial temperature and better mixing.

Solution/melt polymerization starting with 6A6

A disadvantage of using bisester tetraamides in the preparation of the copolymer is the two-step synthesis of the tetraamide unit before the polymerization. A shorter route for obtaining PTMO–T6A6T would be to synthesize T6A6T *in situ* by starting with dia-

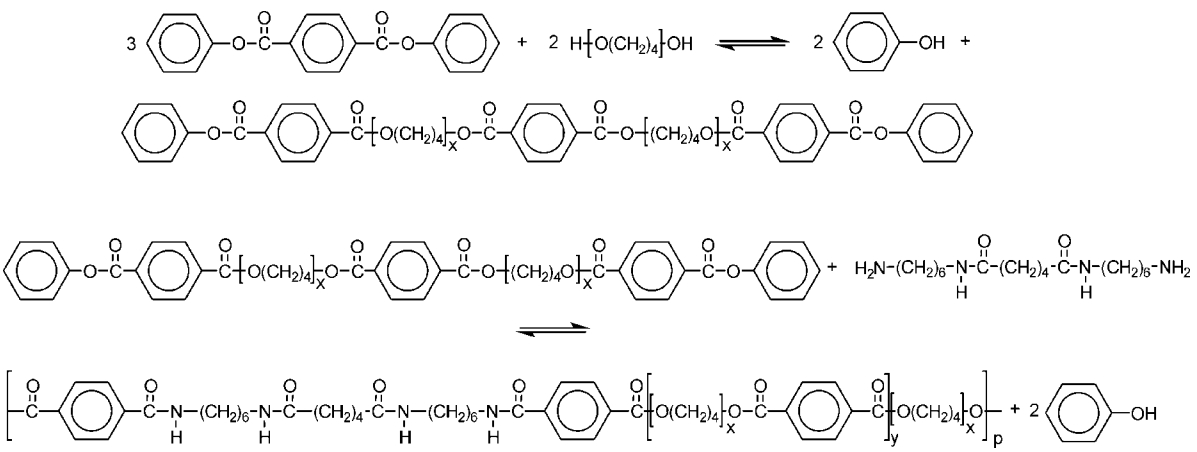

Figure 6 Synthesis of ($PTMO_{1400}$–T)$_{3060}$–T6A6T starting from $PTMO_{1400}$, DPT, and 6A6 (2 : 3 : 1).

TABLE II
Some Properties of $PTMO_x$–T6A6T and $(PTMO_{1000}–T)_y$–T6A6T Copolymers

		T6A6T (wt %)	Inherent viscosity (dL/g)	T_m (°C)	ΔH_m (J/g of T6A6T)	T_c (°C)	$T_m - T_c$ (°C)	X_c by DSC (%)	X_c by FTIR (%)
T6A6T-dimethyl		100	—	255	138	235	20	—	—
Series 1	$PTMO_{650}$	43.8	1.8	200	125	176	24	91	87
	$PTMO_{1000}$	34.2	2.5	191	117	165	26	85	92
	$PTMO_{1400}$	27.1	1.5	188	114	156	28	83	89
	$PTMO_{2000}$	21.1	2.9	183	130	164	19	93	86
	$PTMO_{2900}$	15.7	3.5	—	—	—	—	—	86
Series 2	$PTMO_{1000}$	34.2	2.5	191	117	165	26	85	92
	$(PTMO_{1000}–T)_{4000}$	11.9	1.7	—	—	—	—	—	85
	$(PTMO_{1000}–T)_{6000}$	8.3	1.7	—	—	—	—	—	89
	$(PTMO_{1000}–T)_{8000}$	6.4	1.5	—	—	—	—	—	93
	$(PTMO_{1000}–T)_{10,000}$	5.2	1.8	—	—	—	—	—	81
	$(PTMO_{1000}–T)_{20,000}$	2.7	1.8	—	—	—	—	—	92

mine–diamide 6A6 and reacting it with a terephthalic ester during the polymerization (Fig. 6). The terephthalic ester DPT is suitable for this purpose.[23] Excess DPT was used to minimize the formation of longer amide segments. The copolymer synthesized was $(PTMO_{1400}–T)_{3060}$–T6A6T starting from DPT, $PTMO_{1400}$, and 6A6 with a 3 : 2 : 1 ratio. First, $PTMO_{1400}$ was reacted with DPT to a DPT-end-capped PTMO (DPT–$PTMO_{1400}$–T–$PTMO_{1400}$–DPT), which was subsequently reacted with 6A6. The so-obtained copolymer was colored and not transparent. The opaque appearance suggests that (some) phase separation took place. With this polymerization method, long amide segments can be formed, such as T6A6T6A6T, that are not miscible with PTMO segments and thus phase-separate in the melt, although the contents will be small. The inherent viscosity of the polymer was 1.6 dL/g, which is somewhat lower than that of the copolymer made with T6A6T-dimethyl (Table I). Also, the rubber modulus and T_m are lower, and the CS is higher.

PTMO–T6A6T copolymers can be readily prepared by the three routes discussed previously. However, the copolymers synthesized by the solution/melt route starting from T6A6T-diester displayed the best properties, whereas the melt-synthesized copolymer was the least colored. The color formation is thought to be due to the interaction of NMP and the titanate catalyst. Using another solvent than NMP might limit the color formation. The solvent/melt route was used for the synthesis of the copolymers discussed in the next section.

T6A6T content

In segmented copolymers with crystallizable segments of a constant length, a change in the PTMO length has a direct effect on the amide content.[4,5,13–15,18] Two series of copolymers were prepared, one with $PTMO_x$ segments of various molecular weights (650–2900 g/mol) and one with $PTMO_{1000}$ extended with DMT to $(PTMO_{1000}–T)_y$ with molecular weights up to 20,000 g/mol (Table II).

As the flexible segment length increased, the T6A6T content decreased, from 44 to 16 wt % in the first series and from 34 to 2.7 wt % in the second. The inherent viscosities of the first series increased with the PTMO length, whereas those of the second series were fairly constant. At a particular degree of polymerization, the molecular weight increased faster when longer $PTMO_x$ units were used. The copolymers of both series were transparent in the molten phase, and this indicated that melt phasing did not occur. If in the molten phase two phases were present, then the melt was no longer transparent as a dispersed phase scattered light. At room temperature, the segmented copolymer with a $PTMO_{650}$ (series 1) was opaque, and all other copolymers remained transparent. All the copolymers were easily injection-molded.

DSC

The melting and crystallization behavior of the segmented copolymers was evaluated by DSC (Table II). For the polymers with low concentrations of crystallizable segments (< 16 wt %), no melting or crystallization peaks related to the rigid block could be observed. Thus, for copolymers of the second series, no transition for the T6A6T segment was seen. T_m and T_c of T6A6T from the first series decreased with increasing $PTMO_x$ length (PTMO content). This lowering of the transition temperatures with increasing PTMO content can be described as a solvent effect.[13,24] The difference between the melting peak and the onset of the crystallization peak, normally known as undercooling, is only 20° (Fig. 7). This means that the T6A6T crystallization is extremely

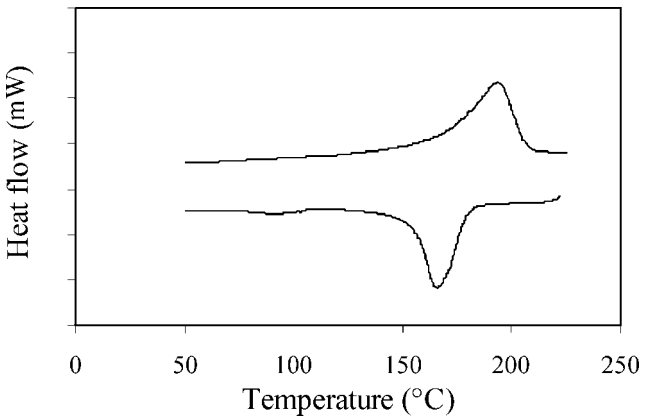

Figure 7 DSC results of $PTMO_{1000}$–T6A6T in heating and cooling.

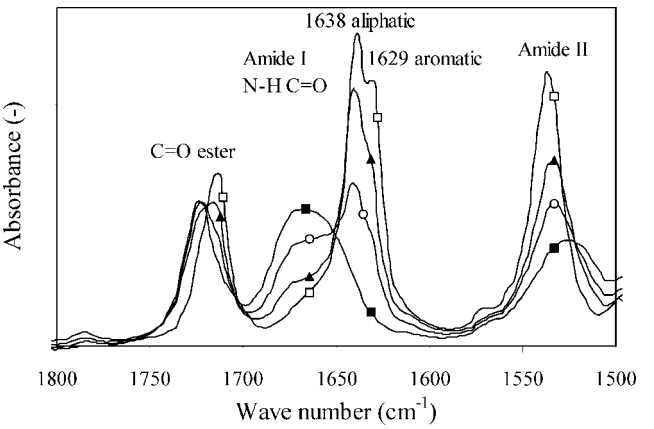

Figure 9 Temperature-dependent FTIR spectra of $PTMO_{1000}$–T6A6T (T_m = 191°C): (□) 25, (▲) 160, (○) 190, and (■) 210°C.

fast. The melting enthalpy, corrected for the actual amount of T6A6T in the samples, is more or less constant at 110–130 J/g, and the degree of crystallinity was calculated with the melting enthalpy of the pure T6A6T (138 J/g; see the Synthesis of T6A6T-dimethyl section). For these segmented copolymers, the crystallinity of the T6A6T segment is high, that is, 80–90%.

FTIR

FTIR is a helpful tool for studying the crystallinity of the amide groups in the polymers. The carbonyl wave number of the amide group shifts to lower values with increasing strength of the hydrogen bonding (Fig. 8). For the amide carbonyl groups of T6A6T in the tightly packed crystalline state, two peaks are observed: one at 1630 cm^{-1} corresponding to the aromatic amide[25] and one at 1640 cm^{-1} corresponding to the aliphatic amide.[21] Similar results have also been observed for T6A6T-dimethyl (Fig. 3). The C=O groups of the amorphous amide have greater interchain distances with, at the same time, a wider variation of distances, thus giving rise to a broad peak at 1670 cm^{-1}. Also present in the figure is the ester carbonyl band at 1710–1720 cm^{-1}. In the solid state, the crystalline amide peaks are strong, and upon heating, the amorphous amide peak increases at the cost of the crystalline bands (Fig. 9).

In the melt, only a broad, amorphous amide carbonyl band is observed. The crystallinity of the T6A6T segments could be calculated from the ratio of the crystalline and amorphous amide peaks [eq. (3)]. For nylon 6,6, this crystallinity obtained by FTIR corresponds according to the crystallinity from the density of the polymer.[26] In Figure 10, the crystallinity of T6A6T in the $PTMO_{1000}$–T6A6T is given as a function of the temperature in a heating and a cooling cycle. The crystallinity of the T6A6T segment was high (92%) at room temperature and remained high up to 150°C. At 170°C, just before the T_m, a sharp decrease in the crystallinity was observed. At

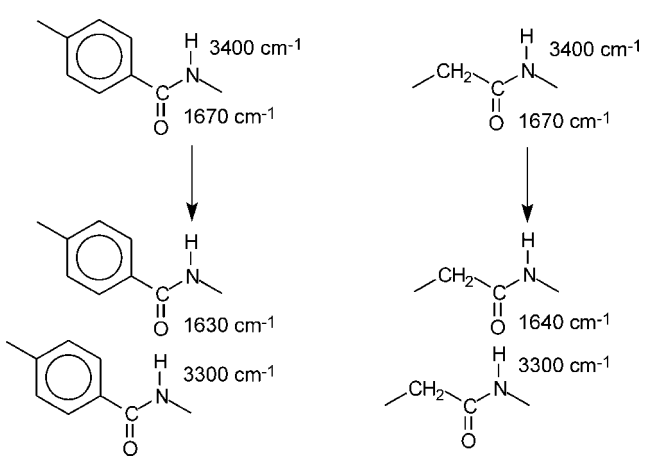

Figure 8 IR absorption bands of aromatic and aliphatic amides.[20,24]

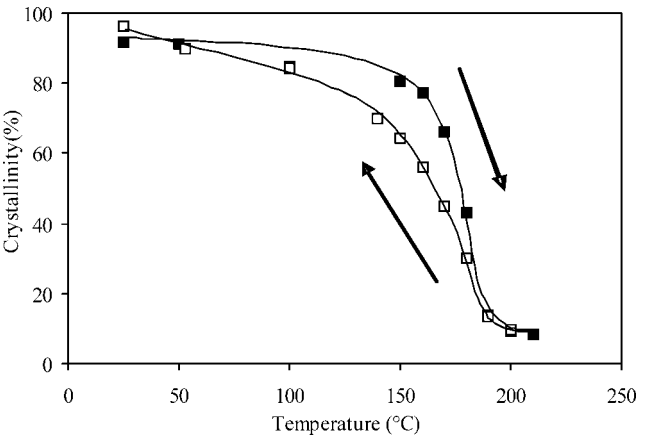

Figure 10 Crystallinity determined by FTIR as a function of temperature for $PTMO_{1000}$–T6A6T: (■) heating curve and (□) cooling curve.

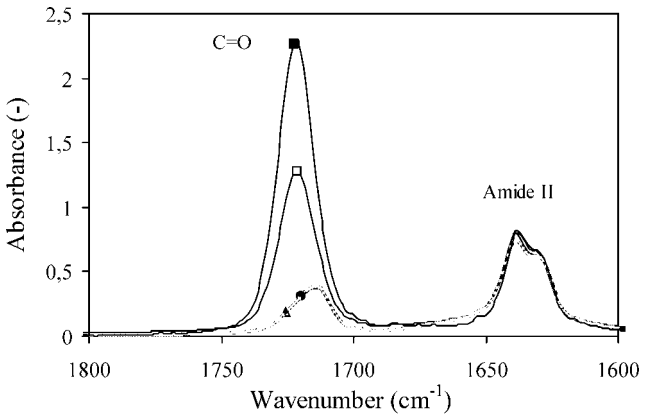

Figure 11 FTIR (1600–1800 cm^{-1}) for (▲) $PTMO_{1000}$–T6A6T, (●) $PTMO_{2000}$–T6A6T, (□) $(PTMO_{1000}–T)_{4000}$–T6A6T, and (■) $(PTMO_{1000}–T)_{8000}$–T6A6T.

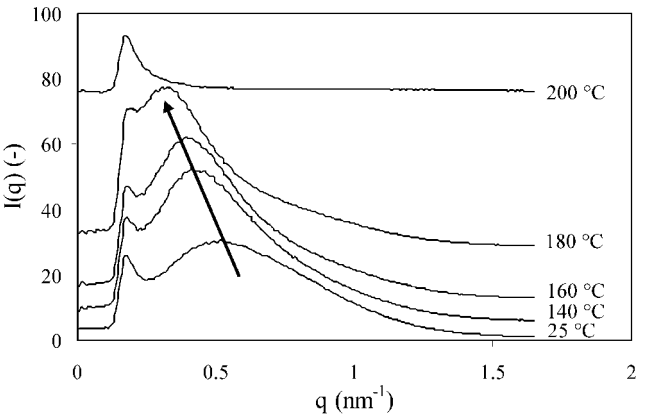

Figure 13 SAXS curves of $PTMO_{1000}$–T6A6T (T_m = 191°C) with increasing temperatures.

even higher temperatures, there was still some crystallinity of the T6A6T segments left. This is possibly due to a small fraction of longer amide segments (e.g., T6A6T6A6T) being present in the copolymer because these have a higher T_m. The cooling cycle shows a similar path as the heating curve and the crystallinity recovered completely. The crystallinities of the other copolymers of this series could be determined in a similar way and were at room temperature all very high (Table II). Thus, even at very low T6A6T contents, the crystallinities could be determined. The crystallinities from FTIR correspond reasonably well with the results from DSC.

In the copolymers of the second series [$(PTMO_{1000}–T)_y$–T6A6T], the $PTMO_{1000}$ is extended with terephthalic ester groups. The FTIR spectra of these copolymers display a stronger ester carbonyl peak (Fig. 11) than that for the copolymer in the first series. This ester carbonyl peak increased with the terephthalic ester content in the PTMO. The T6A6T crystallinity of the copolymers from series 2 could also be determined from the ratio of the crystalline amide (1630 cm^{-1}) and amorphous amide (1670 cm^{-1}) peaks by the use of eq. (3). The value of the factor a in this equation was assumed to be equivalent to that used in series 1, and the results are presented in Table II. The crystallinities of the T6A6T segment in this series are also very high, even for very low T6A6T contents (2.7 wt %).

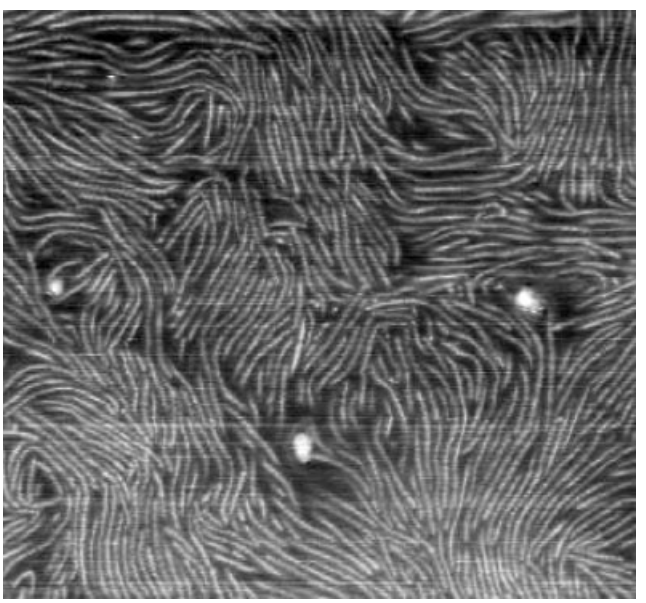

Figure 12 AFM phase image of a $(PTMO_{1000}–T)_{20,000}$–T6A6T solution cast onto a silicon wafer (image size = 1 × 1 μm^2, phase angle = 0–20°).

AFM

The topography of the copolymers was studied by AFM. In the AFM phase-angle mode, the T6A6T crystallites can be distinguished as white ribbons. For samples with high T6A6T contents, the corresponding micrograph was crowded, and with very low T6A6T contents, the ribbons were visible over a wide

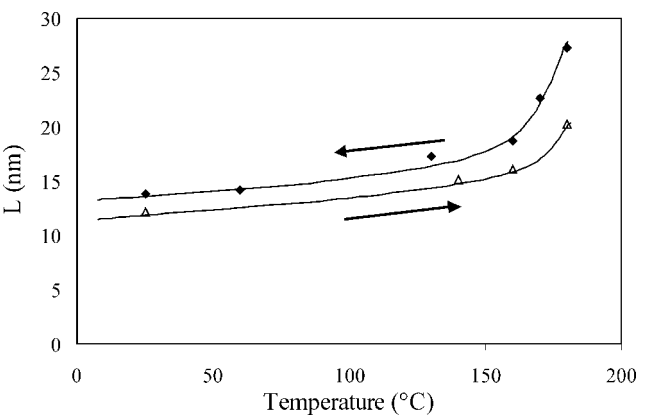

Figure 14 L for $PTMO_{1000}$–T6A6T versus the temperature: (△) heating and (◆) cooling.

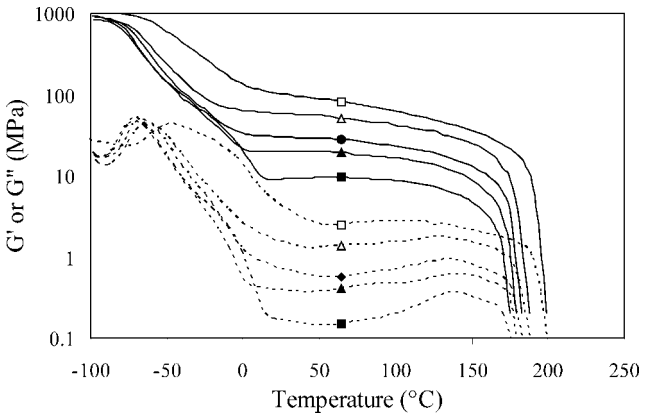

Figure 15 G' and G'' as functions of temperature for $PTMO_x$–T6A6T with PTMOs of various molecular weights: (□) 650, (△) 1000, (●) 1400, (▲) 2000, and (■) 2900 g/mol.

scale (Fig. 12). From the AFM images, an average ribbon thickness of ~ 4–5 nm was measured. This thickness is, however, merely indicative because the dimension of the AFM tip resulted in an inaccurate measure of the thickness. The (visible) lengths of the crystalline ribbons reached values up to 1 μm. The total length of a ribbon could not be measured with AFM as only the morphology at the surface was visible and only part of the ribbon present at the surface was visible. The thickness of the crystalline ribbons is expected to be the extended length of T6A6T, about 3.7 nm, whereas the ribbon widths (the third direction) can vary with heat treatment.[27] Transmission electron microscopy (TEM) measurements of similar copolymers revealed ribbon lengths of 1000–5000 nm.[15,18] Therefore, the aspect ratio of the crystalline ribbons is expected to be about 200–1000.

SAXS

The copolymer $PTMO_{1000}$–T6A6T was analyzed by SAXS in a heating and cooling scan. For the heating scan, the scattering intensity [$I(q)$] plotted versus q (nm) is given (Fig. 13). The background was subtracted from the intensity. The first maximum in the SAXS curve is from the scattering of the beam, and the second maximum of q is related to the interdomain L value.

L of $PTMO_{1000}$–T6A6T at 25°C was 12.2 nm. For ribbonlike morphologies, L is an average of the long spacing in the thickness and in the width direction. The thickness of the crystalline ribbons should correspond to the extended length of the T6A6T units (i.e., 3.7 nm). The crystallite width is of unknown dimensions and probably sensitive to the thermal history of the sample. The length of the ribbons is of the order of 1000–5000 nm. L was found to slightly increase up to 150°C, whereas a significant increase was observed upon melting (Fig. 14).

The monodisperse segments melted in a small temperature range. No long-range order could be observed above the T_m of the segmented copolymer, and this indicated that there was no (liquid) crystalline order present in the molten phase. Upon cooling, the domain spacing nearly returned to its initial value. L of the cooling curve was close to the heating curve, confirming the high rate of crystallization, as was also seen in DSC and FTIR.

The SAXS spectrum of $PTMO_{2000}$–T6A6T displayed a long period of 15.1 nm. This increase in L over $PTMO_{1000}$–T6A6T could be explained by the longer PTMO segment length.

DMTA

Series 1: $PTMO_x$–T6A6T. The thermal mechanical properties of the $PTMO_x$–T6A6T polymers were studied by DMTA. G' and G'' were determined as functions of temperature (Fig. 15). Three transitions were present in the graphs: the glass transition of the PTMO phase, the melting transition of the PTMO, and the melting transition of the T6A6T. The glass transition of the amorphous T6A6T phase, expected at a temperature of 125°C, was not observed. The T_g of the soft phase of $PTMO_x$–T6A6T increased from −70°C for $PTMO_{2900}$ and $PTMO_{2000}$

TABLE III
DMTA Properties of $PTMO_x$–T6A6T with PTMOs of Various Molecular Weights

		T6A6T (%)	T_g (°C)	T_{flex} (°C)	$G'_{25°C}$ (MPa)	T_{flow} (°C)	$\Delta G' \times 10^{-3}$ (°C^{-1})
Series 1	$PTMO_{650}$	43.8	−45	0	102	200	5.0
	$PTMO_{1000}$	34.2	−60	−20	51	185	4.9
	$PTMO_{1400}$	27.1	−65	−15	30	180	4.0
	$PTMO_{2000}$	21.1	−70	0	20	180	2.9
	$PTMO_{2900}$	15.7	−70	10	9	175	1.8
Series 2	$PTMO_{1000}$	34.2	−60	−20	51	185	4.9
	$(PTMO_{1000}–T)_{4000}$	11.9	−63	5	8	165	2.1
	$(PTMO_{1000}–T)_{6000}$	8.3	−63	10	6	160	0.7
	$(PTMO_{1000}–T)_{8000}$	6.4	−62	15	4	150	0.7
	$(PTMO_{1000}–T)_{10,000}$	5.2	−60	15	3	150	1.7
	$(PTMO_{1000}–T)_{20,000}$	2.7	−62	15	1.6	130	1.8

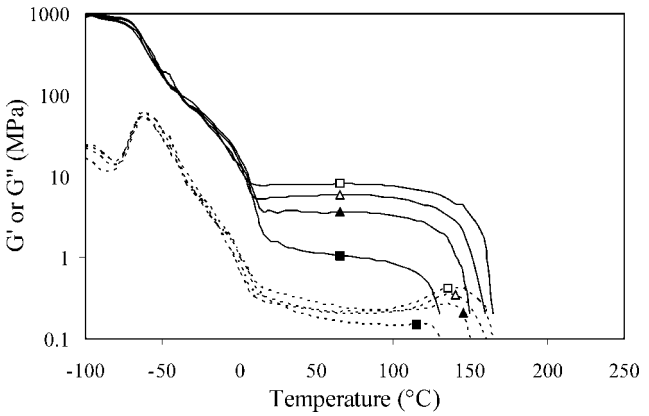

Figure 16 G' and G'' as functions of temperature for $(PTMO_{1000}–T)_x$–T6A6T with various values of x: (□) 4000, (△) 6000, (▲) 10,000, and (■) 20,000 g/mol.

to −45°C for $PTMO_{650}$ (Table III). This increase in T_g was due to the increase in the density of the physical crosslinks.[18,28] The low T_g values for $PTMO_{2900}$- and $PTMO_{2000}$-based polymers indicated that the concentration of T6A6T segments in the polyether phase must be very low.

The T_m of the PTMO phase was identified as a shoulder on the G' and G'' curves in the DMTA graph (Fig. 15). A PTMO T_m was present for samples with PTMO lengths of at least 1400 g/mol and ranged between 5 and 10°C. T_{flex}, defined as the start of the rubber plateau, was increased as a result of the crystalline PTMO phase and varied from −20 to 10°C. The values of T_{flex} for $PTMO_{650}$ and $PTMO_{1000}$ were low because of the low PTMO T_m and crystallinity. T_{flex} is also influenced by T_g, and this effect can clearly be seen with $PTMO_{650}$, which had somewhat higher values.

The copolymers had rubber moduli that were almost temperature-independent, and this is typical for copolymers with crystallizable segments of monodisperse lengths.[4–18,29] The change in the rubber modulus as a function of temperature could be quantified with $\Delta G'$ [eq. (6), Table III]; a high value of $\Delta G'$ indicated a modulus that was strongly dependent on the temperature. The $\Delta G'$ values decreased slightly with increasing PTMO length, thus suggesting better developed crystalline structures at low T6A6T contents. The monodisperse segments in these copolymers are expected to form crystalline ribbons with uniform thicknesses, giving rise to a well-defined T_{flow}. The T_{flow} values correspond well to the T_m values recorded with DSC (Table II).

Series 2: $(PTMO_{1000}–T)_x$–T6A6T. The thermal mechanical properties of $(PTMO_{1000}–T)_y$–T6A6T are listed in Table III and shown in Figure 16. Even at a very low T6A6T concentration (2.7 wt %), the segmented copolymer has a rubber plateau and a high T_{flow}. The T_g values of the copolymers in this series are similar, suggesting that the extension of $PTMO_{1000}$ with terephthalate has little effect on the T_g or phase separation. The T_{flex} values increase somewhat with increasing $(PTMO_{1000}–T)_y$ length, indicating increased PTMO crystallization. This is believed to be an effect of the decreased network density. All copolymers have a virtually temperature-independent rubber modulus between T_{flex} and T_{flow}.

$G'_{25°C}$ for the copolymers of series 1 and 2 decreases drastically with increasing length of the flexible segment [$PTMO_x$ and $(PTMO_{1000}–T)_y$] and thus decreasing amide content (Fig. 17). This significant change in the modulus is partly due to the changing crosslink density but is mainly a result of the reinforcing effects of the rigid-segment crystallites.[15,18] The reinforcing effect of the crystallites is a function of the crystalline content and the aspect ratio of these crystallites. The aspect ratio of the T6A6T crystallites in these copolymers is high (Fig. 12).

There exist many mechanical models that describe the modulus of a composite as a function of the filler content.[26,30–32] With the Halpin–Tsai model, the elastic modulus of a fiber composite with randomly oriented fibers as a function of the fiber content and aspect ratio is calculated.[29–30] The Halpin–Tsai model has also been applied to semicrystalline polymers[31] and segmented block copolymers,[15,18] and has been chosen for the systems in this study. In this calcula-

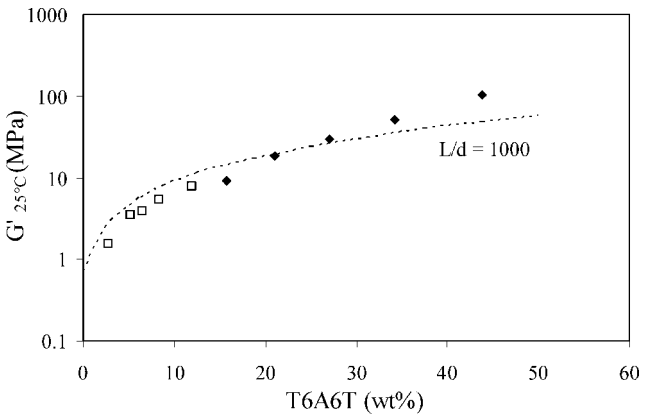

Figure 17 G' versus the amide weight percentage: (◆) series 1 ($PTMO_x$–T6A6T), (□) series 2 [$(PTMO_{1000}–T)_y$–T6A6T], and (- - -) Halpin–Tsai relation ($L/D = 1000$).

TABLE IV
Parameters Used in the Halpin–Tsai Model

G_s	Modulus of the PTMO matrix (extrapolated from Fig. 17)	0.8 MPa
E in H-bonding direction	$E_\perp$ of Kevlar[29]	5000 MPa
v_c	Poisson ratio (Kevlar)[29]	0.35
L/D	Aspect ratio (TEM)[15]	1000

tion, it was assumed that the crystallinity of the amide segments was 88%. The following parameters were used for the calculation of the modulus: the modulus of the matrix polymer (PTMO), the modulus of the reinforcing phase (crystalline amide), the crystalline content, and the aspect ratio of the crystallites (Table IV). A detailed description of the calculation can be found elsewhere.[33]

The increase in the modulus as described by the Halpin–Tsai model with Youngs modulus (E modulus) for the crystallites of 5 GPa and an aspect ratio of 1000 fit reasonably well with the experimental results (Fig. 17). The strong increase in the modulus with the amide content of the segmented block copolymers can be explained by the high amide crystallinity and the high aspect ratio of the crystallites.

The flow (melt) transitions of the T6A6T segments in the copolymers were sharp and decreased in temperature with increasing lengths of the flexible segments. This lowering of T_{flow} can be explained with the solvent effect, as proposed by Flory[34] for random copolymers, which seems to be applicable too for block copolymers.[13,24]

CONCLUSIONS

T6A6T is an interesting crystallizable segment for segmented block copolymers as its T_m is not particularly high. Three routes of copolymer synthesis were studied: a melt polymerization; a combined solvent/melt polymerization; and a synthesis route starting with PTMO, 6A6-diamine, and DPT. All routes resulted in polymers with high molecular weights. $PTMO_x$–T6A6T copolymers prepared with T6A6T-dimethyl units by the solution/melt procedure had the best properties with respect to the modulus and a lower CS, but the other routes were simpler.

The influence of the flexible segment length was studied by the variation of the $PTMO_x$ length and by the use of extended $PTMO_{1000}$ [$(PTMO_{1000}–T)_y$]. The concentration of T6A6T was thereby decreased from 44 to 2.7 wt %. The crystallinity of the T6A6T segments in the copolymers, as studied by DSC and FTIR, was very high ($\sim$ 88%). Even the copolymers with extremely low T6A6T contents (2.7 wt %) had a high T6A6T crystallinity. The crystallinity measured with temperature-dependent FTIR remained high up to the T_m of the copolymer. The crystallization curve of the rigid segments upon cooling resembled the one obtained upon heating, indicating a fast crystallization of the tetraamide segments.

The T6A6T crystallites had a nanoribbon structure with an expected thickness of about 4 nm and a length of $>$ 1000 nm. L, as determined by SAXS, was for $PTMO_{1000}$–T6A6T 12.2 nm and for $PTMO_{2000}$–T6A6T 15.1 nm. On the heating of the segmented copolymer, L, as measured by SAXS, was maintained up to the T_m, indicating the presence of stable crystallites that, on cooling, returned to their initial value.

The copolymers had low T_g values suggesting a good phase separation of the ether and amide segments. The flexible segments were either $PTMO_x$ or $(PTMO_{1000}–T)_y$. Increasing the flexible segment length increased T_{flex} as a result of the increasing PTMO T_m. This increase was stronger for $PTMO_x$ than for $(PTMO_{1000}–T)_y$. The modulus at room temperature increased significantly with the amide content, and this strong increase could be explained by a composite model describing the reinforcement with fibers.

The authors thank the European Synchrotron Radiation Facility at Grenoble, France, for the use of its facilities and Brass and Heunen for their assistance.

References

1. Holden, G.; Legge, N. R.; Quirk, R.; Schroeder, H. E. Thermoplastic Elastomers, 2nd ed.; Hanser: Munich, 1996.
2. Fakirov, S. Handbook of Condensation Thermoplastic Elastomers; Wiley-VCH: Weinheim, 2005.
3. Dreyfuss, P. Polytetrahydrofuran; Polymer Monographs 8; Gordon & Breach: New York, 1982.
4. Niesten, M. C. E. J.; ten Brinke, J. W.; Gaymans, R. J. Polymer 2001, 42, 146.
5. Krijgsman, J.; Husken, D.; Gaymans, R. J. Polymer 2003, 44, 7573.
6. Allegrezza, A. E.; Seymour, R. W.; Ng, H. N.; Cooper, S. L. Polymer 1974, 15, 433.
7. Harrel, L. L. Macromolecules 1969, 2, 607.
8. Ng, H. N. Polymer 1973, 14, 255.
9. Eisenbach, C. D.; Baumgartner, M.; Gunter, G. In Advances in Elastomer and Rubber Elasticity; Lal, J.; Mark, J. E., Eds.; Proceedings Symposium; Plenum: New York, 1985; p 51.
10. Heijkants, R. G. J. C.; van Calck, R. V.; van Tienen, T. G.; de Groot, J. H.; Buma, P.; Pennings, A. J.; Veth, R. P. H.; Schouten, A. J. Biomaterials 2005, 26, 4219.
11. Versteegen, R. M.; Sijbesma, R. P.; Meijer, E. W. Macromolecules 2005, 38, 3176.
12. van der Schuur, J. M.; Noordover, B.; Gaymans, R. J. Polymer 2006, 47, 1091.
13. Husken, D.; Krijgsman, J.; Gaymans, R. J. Polymer 2004, 45, 4837.
14. Gaymans, R. J.; de Haan, J. L. Polymer 1993, 34, 4360.
15. van der Schuur, J. M.; de Boer, J.; Gaymans, R. J. Polymer 2005, 46, 9243.
16. Rabani, G.; Rosair, G. M.; Kraft, A. J Polym Sci Part A: Polym Chem 2004, 42, 1449.
17. Yamakawa, H.; Miyara, H. In Handbook of Condensation Thermoplastic Elastomers; Fakirov, S., Ed.; Wiley-VCH: Weinheim, 2005; Chapter 5.
18. van der Schuur, J. M.; Gaymans, R. J. J Polym Sci Part A: Polym Chem 2006, 44, 4769.
19. Krijgsman, J.; Husken, D.; Gaymans, R. J. Polymer 2003, 44, 7043.
20. Morgan, P. W. Condensation Polymers; Polymer Reviews 10; Interscience: New York, 1965; Appendix B, p 469.
21. Dechant, J. Ultrarot-Spektroskopische Untersuchungen an Polymeren; Maxim Gorki: Berlin, 1972.
22. Costa, L.; Luda, M. P.; Cameron, G. G.; Qureshi, M. Y. Polym Degrad Stab 2000, 67, 527.

23. Lohmeijer, J. H. G. M.; Banach, T. E.; Brunelle, D. J.; Hoogland, G.; Faber, R. U.S. Pat. 6,054,552 (2000).
24. Niesten, M. C. E. J.; Feijen, J.; Gaymans, R. J. Polymer 2000, 41, 8487.
25. Gaymans, R. J. J Polym Sci 1985, 23, 1599.
26. Zbinden, R. Infrared Spectroscopy of High Polymers; Academic: New York, 1964.
27. Nielsen, L. E. J Macromol Sci Rev Macromol Chem 1969, 3, 69.
28. Eisenbach, C. D.; Stadler, E.; Enkelmann, V. Macromol Chem Phys 1995, 196, 833.
29. Peacock, A. J. Handbook of Polyethylene; Marcel Dekker: New York, 2000.
30. Halpin, J. C.; Kardos, J. L. J Appl Phys 1972, 43, 2235.
31. Hiemenz, P. C. Polymer Chemistry; Marcel Dekker: New York, 1984.
32. McCrum, N. G.; Buckley, C. P.; Bucknall, C. B. Principles of Polymer Engineering, 2nd ed.; Oxford University Press: New York, 2001.
33. van der Schuur, J. M. Thesis, University of Twente, 2004; Appendix A, p 195.
34. Flory, P. J. Trans Faraday Soc 1955, 51, 848.